Reaction Chemistry & Engineering

ROYAL SOCIETY OF CHEMISTRY

PAPER

View Article Online
View Journal | View Issue

Check for updates

Cite this: *React. Chem. Eng.*, 2026, **11**, 106

Heterogeneous catalytic epimerization of D-glucose to D-mannose by a tin-organic framework

Valérie Toussaint, [a] Loretta Pavlis,[a] Pia Groß, [a] Samantha F. Ausman,[b] Susannah L. Scott, [b] Karin Föttinger [c] and Irina Delidovich [a]*

Received 18th July 2025,
Accepted 16th September 2025

DOI: 10.1039/d5re00314h

rsc.li/reaction-engineering

Monosaccharide D-mannose (D-Man) is of great interest in the food and pharmaceutical industries as a low-calorie sweetener and precursor for D-mannitol and medicaments. Nowadays, large-scale production of D-Man remains challenging due to a lack of efficient chemo-catalytic processes using D-glucose (D-Glc) as educt. In this work, heterogeneous catalytic epimerization of D-Glc to D-Man by a tin-organic framework (Sn-OF-1) was achieved. The reaction kinetics were explored using both conventional methods and time-resolved *operando* MAS ^{13}C NMR spectroscopy. Under optimized reaction conditions (100 °C, 5 wt% D-Glc, 20 mg(cat) g^{-1}(EtOH : H_2O)), epimerization yielded a 77 : 23 equilibrium mixture of D-Glc : D-Man after 1.5 h reaction time. Most D-Glc (*ca.* 73%) was recovered from the obtained mixture of saccharides by crystallization from EtOH : MeOH (4.7 : 1). The remaining mixture of D-Man and D-Glc was separated *via* adsorption on CaY zeolite, resulting in a stream containing D-Man at 70% purity.

Open Access Article. Published on 17 September 2025. Downloaded on 2/13/2026 12:00:53 PM.
This article is licensed under a Creative Commons Attribution 3.0 Unported Licence.

1. Introduction

Processing of biomass-derived feedstocks is expected to expand in the near future, driven in part by the growing demand for specialty monosaccharides in the food and pharmaceutical industries. In this regard, the production of D-mannose (D-Man) is of considerable interest. D-Man can serve as a low-calorie sweetener, being 0.60 and 0.86 times as sweet as sucrose and D-glucose (D-Glc), respectively.[1,2] It is also a precursor for antitumor and immunostimulating agents.[1] Additionally, D-Man can be converted to D-mannitol, valued for its dental benefits and low hygroscopicity.[1,3] D-Mannitol is industrially produced by hydrogenation of D-fructose-containing syrups, often a 1 : 1 mixture of D-glucose and D-fructose yielding a 1 : 3 mixture of D-mannitol and D-sorbitol.[4] Therefore, efficient and cost-effective large-scale production methods for pure D-Man, both in its own right and as a direct precursor for D-mannitol, could be industrially important.

Traditional extractions of D-Man from biomass components such as hemicelluloses or mannans *via* acid hydrolysis require large amounts of organic reagents and high temperatures. Enzymatic hydrolysis can be conducted under milder conditions, but face challenges such as enzyme deactivation and long reaction times, hindering commercial scalability.[1,2,5] Chemo-catalytic epimerization of D-Glc could be a more efficient method for producing D-Man. The highly efficient homogeneous molybdate catalysts discovered by Bilík accomplish this epimerization, resulting in a 75 : 25 mixture of D-Glc to D-Man.[6] Formation of D-Man from D-Glc in 17% yield in a phosphate buffer solution under subcritical conditions was reported.[7] Homogeneous catalysis poses challenges for catalyst recycling and reuse. In heterogeneous systems, Kegging-type phosphomolybdate catalysts[8] and commercial zeolite support molybdenum[9] enable *ca.* 32.5% yield of D-Man with 94% selectivity. Although several solid molybdenum-based catalysts were developed, high leaching is observed, leading to low long-term stability and reduction of the active Mo species.[10–12] In the presence of solid Ca–Al mixed oxides, 65% D-Man yield at 73% selectivity was reported. However, the mixed oxides exhibit leaching of the metal species, promoting degradation of

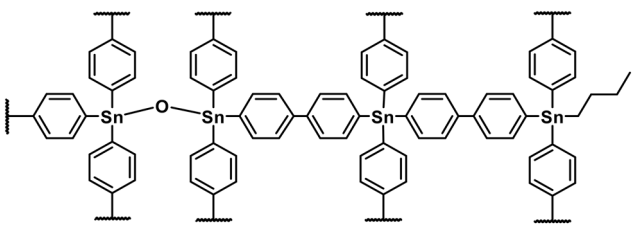

Fig. 1 Structure of Sn-OF-1.[20]

[a] *Institute of Chemical, Environmental and Bioscience Engineering, TU Wien, Getreidemarkt 9, 1060 Vienna, Austria. E-mail: irina.delidovich@tuwien.ac.at*
[b] *Department of Chemistry & Biochemistry and Department of Chemical Engineering, University of California, Santa Barbara, California 93106, USA*
[c] *Institute of Materials Chemistry, TU Wien, Getreidemarkt 9, 1060, Vienna, Austria*

This journal is © The Royal Society of Chemistry 2026

Open Access Article. Published on 17 September 2025. Downloaded on 2/13/2026 12:00:53 PM.
This article is licensed under a Creative Commons Attribution 3.0 Unported Licence.

monosaccharides.[13] Porous tin-organic frameworks (Sn-OFs)[5,6,11,14–18] with Lewis acidic Sn^{4+} sites connected by organic linkers *via* covalent tin-carbon bonds (Fig. 1) catalyze heterogeneous epimerization. For example, Delidovich *et al.* reported that hydrophobic Sn-OFs epimerize D-Glc to D-Man with 21% yield and 91% selectivity in a water-ethanol mixture.[19] Sn-OFs catalyze efficient epimerization in water–ethanol solvent, with very low leaching of tin and minor structural changes during reaction. Results of the hot-filtration test support that Sn-OFs catalyzed the epimerization of D-Glc into D-Man heterogeneously.[19] The structure of the Sn-OFs was comprehensively examined in the previous work.[20] Sn-OFs also show high potential for epimerization of different substrates to produce rare sugars such as L-ribose, D-talose, D-lyxose, and L-quinovose with selectivities ranging from 67–95%.[21]

Separation of the resulting mixtures of D-Glc and D-Man presents a challenge.[22] Purification of sugars is commonly achieved using ion chromatography (IC), generally performed with a cation-exchange resin and water as the mobile phase,[23,24] but requires long columns and large amounts of eluent.[19] Separation on cation exchange resins occurs due to formation of bidentate complexes (*ax–eq*) with alkaline earth cations ($K_{compl.}$ = 0.1 mol^{-1} in water) or, possibly, more stable tridentate complexes (*ax–eq–ax*) ($K_{compl.}$ = 1–5 mol^{-1} in water). CaY zeolites with large pores and high Ca^{2+} ion contents in the α-cages facilitate D-Man separation *via* complexation.[25] In previous studies of chromatographic separation of sugars over sulfonated resins in their Ca^{2+} forms, bidentate coordination was suggested (Fig. 2).[26,27] In addition, the β-D-mannopyranoside isomer ($^1C_4$) can form a tridentate complex with Ca^{2+} *via* its *ax–eq–ax* OH groups. Since D-Man has a higher number of *ax–eq* OH-groups that can coordinate to Ca^{2+}, adsorptive separation over CaY zeolites is a promising alternative to chromatography over ion-exchange resins for purifying D-Glc/D-Man mixtures.

Zeolites have been considered less frequently for separation of saccharides than ion-exchanged resins. Chromatography using zeolites as stationary phases was addressed for separation of D-Glc and D-Fru,[28–30] a mixture of glucose-sucrose-sorbitol,[31] or fructose oligosaccharides.[32] Selective adsorption of sucrose on FAU-type zeolites was reported.[33] The group of Buchholz systematically explored adsorption of sugars on zeolites of various frameworks and with different Al : Si ratios.[34,35] Adsorption on KX zeolite was proposed for recovery of D-Glc from an aqueous ionic liquid.[36] More recently, efficiency of BaX and BaY zeolites as adsorbents for separation of D-Glc and D-xylose was reported.[37] Importantly, separation of D-Glc and D-Man has been rarely addressed. For instance, Sherman *et al.* reported the highest efficiency of CaY, BaX, and BaY zeolites as stationary phase for column separation of D-Glc and D-Man using aqueous eluent.[38] To our knowledge, the influence of solvent on adsorption of D-Glc and D-Man onto zeolites has not been reported yet.

This study addresses the conversion of D-Glc to D-Man catalyzed by Sn-OF-1, describing the reaction kinetics and the separation of the resulting equilibrium mixture to recover the D-Man and recycle the D-Glc component.

2. Experimental

2.1. Chemicals

D-Glucose (>99.5%), NaY zeolite, *n*-BuLi (2.5 M in hexane), 4,4′-dibromobiphenyl, Dowex® 66 free base, anhydrous THF (99.9%), $SnCl_4$ (98%), ethanol (>99.8%), 1-^{13}C-D-glucose (99%), tetraphenyltin ($SnPh_4$), and triphenyltin hydroxide

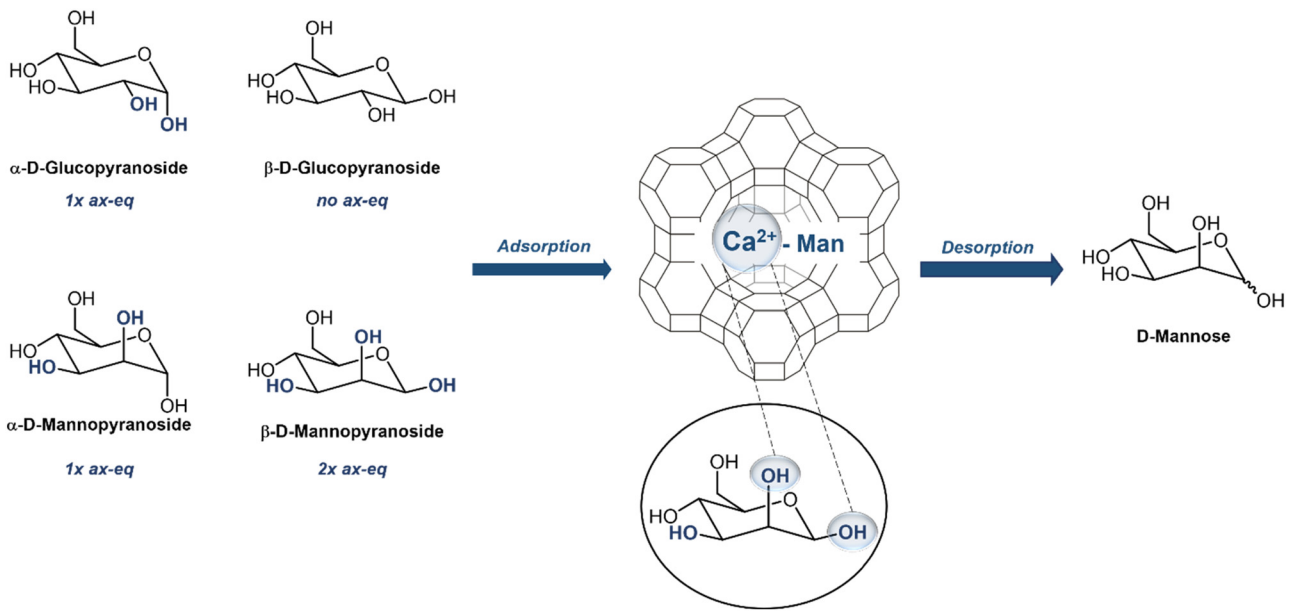

Fig. 2 Separation of D-Man *via* Ca^{2+} complexation in CaY zeolite.

Open Access Article. Published on 17 September 2025. Downloaded on 2/13/2026 12:00:53 PM. This article is licensed under a Creative Commons Attribution 3.0 Unported Licence.

(Ph_3SnOH) were purchased from Sigma Aldrich. D-Mannose (>99%) was obtained from Acros Organics. $CaCl_2$ (97%) and tetrahydrofuran (99.8%) were obtained from Fisher Scientific. Amberlyst® 15 (hydrogen form) was purchased from Supelco. Bis(triphenyltin) oxide ($(Ph_3Sn)_2O$) was synthesised as previously described.[20]

2.2. Characterization

X-ray diffraction (XRD) analysis was conducted on a PANalytical MPD Pro with a Cu tube, a BBHD mirror, 0.04 rad Soller collimator, and $\frac{1}{2}$° divergence slit. An accelerator detector was used in scanning line mode for scans between 4 and 80° with a step size of 0.0201° and a counting time of 80.010 s per point. HighScore software was used for analysis.

N_2 physisorption isotherms were recorded on a Micromeritics ASAP 2060 at 77 K, after degassing samples at 120 °C under vacuum for 24 h. Brunauer–Emmett–Teller (BET) and *t*-Plot models were used to determine surface areas. Micropore analysis was performed using the MicroActive software.

Scanning electron microscopy (SEM) images were acquired using a COXEM EM-30AX, with voltages of 5–15 kV. Samples were coated with Au using a COXEM sputter at 9 mA for 200 s.

X-ray fluorescence (XRF) was carried out on a PANalytical Axios. Samples were mixed with Ultra-Wax and pressed into pellets for analysis.

Adsorbed pyridine was used to characterize acid sites. Sn-OF-1 and each of the model tin compounds (Ph_4Sn, Ph_3SnOH and $(Ph_3Sn)_2O$) at 70 °C were heated under high vacuum (0.001 mbar) overnight at 120 °C before pyridine adsorption was carried out under static vacuum (5–10 mbar). The desorption was performed by applying a high vacuum of 0.001 mbar. IR spectra were recorded on a Vertex 70 FT-IR spectrometer equipped with an MCT detector (resolution 4 cm^{-1}). Samples were prepared as self-supporting wafers (2 cm diameter, typically 7–8 mg cm^{-2}).

2.3. Synthesis of Sn-OF-1

Sn-OF-1 was synthesized as previously reported.[19] In brief, 4,4′-dibromobiphenyl (3.12 g, 10 mmol) was dissolved in anhydrous THF (200 mL). *n*-BuLi (8.0 mL, 20 mmol) was added dropwise while cooling the solution at −10 °C, then the solution was stirred for 30 min at −10 °C. $SnCl_4$ (0.58 mL, 5.0 mmol) was added and stirring was continued for 30 min at −10 °C. The solution was allowed to warm slowly to room temperature, then stirred overnight. The white precipitate was filtered, and the solid was washed two times each with THF (200 mL), H_2O (200 mL), and EtOH (200 mL). The solid was dried under high vacuum to give Sn-OF-1 as a white powder (96% yield, 2.02 g).

2.4. Catalytic tests and analysis of the liquid fraction

Catalytic epimerization was conducted in 9 mL pressure tubes, each containing 100 mg Sn-OF-1 and 5 mL D-Glc or D-Man solution in 50 : 50 wt% EtOH : H_2O. The reaction was initiated by placing the tubes in a pre-heated oil bath and stirring at 750 rpm. After the experiment, the tubes were cooled in an ice bath, then the reaction mixtures were filtered through a PTFE syringe filter (20/25), and the pH of the samples was measured with a pH electrode (WTW). Prior to HPLC analysis, samples were diluted 10-fold, stirred twice with Amberlyst® 15 (hydrogen form, 400 mg, 30 min) and Dowex® 66 free base (1000 mg, 60 min), then filtered again. HPLC analysis to quantify D-Glc, D-Man, and D-Fru was performed on an Agilent 1200 system with an RID detector and a COSMOSIL Sugar-D column (4.6 mm I.D. × 250 mm). The column was operated at 30 °C with an 80 : 20 v% acetonitrile eluent at 1 mL min^{-1}.

2.5. Time-resolved *operando* MAS NMR spectroscopy

Epimerization of 1-^{13}C-D-Glc was monitored using *operando* Magic Angle Spinning (MAS) NMR spectroscopy on a Bruker Avance NMR spectrometer equipped with an 11.7 T magnet and a triple resonance probe operating at 125.7788 MHz for ^{13}C and 500.2185 MHz for ^{1}H. In a typical setup, 9.4 mg Sn-OF-1, 90 mg H_2O, 90 mg EtOH, and 25 mg 1-^{13}C-D-Glc were placed in a 7.5-mm rotor (0.4 mL volume) equipped with Viton o-rings. This ratio of sugar to liquid was chosen to achieve a viscous mixture to ensure rotor stability during spinning with enough liquid for molecular mobility.[39,40] After heating and establishing a stable 3 kHz MAS rate, quantitative ($5 \times T_1$) ^{13}C MAS NMR spectra were recorded, acquiring 8 scans per spectrum. In ^{13}C direct polarization experiments, a 35 kHz ^{1}H decoupling field was used. The acquisition time was 30 ms for ^{13}C, with a spectral width of 50 kHz. ^{13}C chemical shifts were referenced to adamantane (38.5 ppm). Time-resolved NMR spectra were recorded over 5–6 h at 73, 83, 88, and 92 °C. Relative concentrations of D-Glc and D-Man were determined *via* signal integration. To estimate rate constants at each temperature, time-dependent changes were modeled by fitting a system of ordinary differential equations using nonlinear least-squares regression in Python.

2.6. Preparation of CaY zeolite and adsorption/desorption tests

Ion exchange of NaY zeolite. Na^+ ions in NaY zeolite (15 g) were exchanged with Ca^{2+} by stirring the zeolite with a 0.2 M $CaCl_2$ solution (300 mL) at 50 °C for 2 h in a 500 mL round-bottom flask. The solid was removed by centrifuge, washed four times with deionized water (200 mL) before drying in an oven at 80 °C overnight. The ion-exchange procedure was repeated once more. Approximately 77% of Na^+ were substituted by Ca^{2+}. The elemental composition of the CaY zeolite before and after exchange was determined by XRF analysis.

Adsorption–desorption experiments. Time-dependent adsorption curves were recorded for D-Glc and D-Man (50 mg g^{-1} sugar solution, 21 mL) in CaY zeolite (3.5 g). Various solvent mixtures (pure H_2O, and EtOH : H_2O, 50 : 50 and 70 : 30 wt%) were screened. Each solution was stirred while aliquots were removed for analysis at 0, 1, 2, 4, 6, 8, 10,

 This journal is © The Royal Society of Chemistry 2026

Open Access Article. Published on 17 September 2025. Downloaded on 2/13/2026 12:00:53 PM. This article is licensed under a Creative Commons Attribution 3.0 Unported Licence.

and 15 min. Adsorption isotherms were recorded for D-Glc and D-Man individually as well as their mixtures. To record the adsorption isotherms, CaY zeolite (500 mg) and 3 mL of the respective solution were stirred for 2 h at RT. Sugar concentrations in the range of 1 to 50 mg g^{-1} were screened. CaY zeolite was separated from the solution by filtration through a PTFE syringe filter (0.22 μm) and the supernatant was diluted for HPLC analysis.

CaY zeolite (500 mg) was used to adsorb D-Glc or D-Man (50 mg g^{-1}) in 70 : 30 wt% EtOH : H_2O (3 mL) at 500 rpm for 2 h at RT. After adsorption, the zeolite was separated *via* filtration through a PTFE filter (0.22 μm) and either directly desorbed or dried at 80 °C before desorption. Desorption was conducted in 3 mL water at RT upon stirring at 500 rpm for 1 h.

For competitive desorption experiments, sugars from a solution of D-Glc (60 mg g^{-1}) and D-Man (30 mg g^{-1}) in a 67 : 33 ratio were adsorbed by CaY zeolite (500 mg) suspended in EtOH : H_2O (70 : 30 wt%). The zeolite was filtered then rinsed twice with water (3 mL). Sugars were desorbed by stirring with 3 mL water at 500 rpm and RT. Amounts of adsorbed and desorbed sugars were quantified by HPLC.

2.7. Synthesis and recovery of D-Man

Epimerization of D-Glc to D-Man catalyzed by Sn-OF-1. The catalytic experiment was conducted in a 50 mL round-bottom flask containing Sn-OF-1 (800 mg) and a D-Glc solution (40 g, 5 wt% in a 50 : 50 wt% EtOH : H_2O mixture). The reaction was initiated by heating the flask in a pre-heated oil bath at 100 °C while stirring at 750 rpm for 1.5 h. The flask was then cooled in an ice bath and the solution was filtered through a PTFE syringe filter (20/25). Prior to the HPLC analysis, ionic species were removed from the solution using the previously reported method.[41] The resulting sugar solution was stirred twice with Amberlyst® 15 (hydrogen form, 400 mg, 30 min) and Dowex® 66 (free base, 1000 mg, 60 min). Finally, the solution was filtered through a syringe filter (PA 20/25).

Partial crystallization of D-Glc. The reaction solution resulting from epimerization catalyzed by Sn-OF-1 was freeze-dried to yield a sugar syrup. This syrup was dissolved in a mixture of ethanol (4.25 g) and methanol (0.9 g) by heating the solution at 70 °C for 15 min. Seed crystals of D-Glc were added, and the solution was allowed to stand at RT for one week. The crystallized sugar was separated from the solution by decantation, then washed with ethanol and dried under vacuum to obtain purified D-Glc.

Epimerization of crystallized D-Glc. Crystallized D-Glc recovered from the reaction solution was subjected to further epimerization using Sn-OF-1. A solution of D-Glc (3 g, 5 wt%) in a mixture of EtOH and H_2O (50 : 50 wt%) containing Sn-OF-1 (60 mg) was heated at 100 °C for 1.5 h while stirring at 750 rpm. After reaction, the solution was filtered using a PTFE 20/25 syringe filter. D-Glc conversion and D-Man formation were quantified by HPLC. Before analysis, the product mixture was diluted and treated twice with Amberlyst® 15 (hydrogen form, 400 mg, 30 min) and Dowex® 66 (free base, 1000 mg, 60 min), followed by filtration through a PA 20/25 syringe filter.

Recovery of D-Man using CaY zeolite. After crystallization, the remaining EtOH : MeOH solution was removed using a rotary evaporator to yield a sugar syrup. This syrup was dissolved in a 70 : 30 mixture of ethanol (3.5 g) and water (1.5 g). CaY zeolite (500 mg) was added, and the mixture was stirred at RT for 2 h at 500 rpm. The zeolite was separated *via* filtration on a frit. The sugar-containing zeolite was rinsed twice with 3 mL water then stirred in 3 mL water for 1 h at 500 rpm and RT to desorb the sugar.

3. Results and discussion

3.1. Characterization of Sn-OF-1

Sn-OF-1 is an X-ray amorphous micro-/mesoporous material[19] with a specific surface area S_{BET} of 399 m^2 g^{-1} and a pore volume $V_{t\text{-Plot}}$ of 188 cm^3 g^{-1} (Fig. S1). SEM analysis reveals a dendritic network of flat and rod-like particles with an average size of 300–400 nm (Fig. S2).

Our recent study suggested that the network consists mainly of tetraaryltin Ar_4Sn structural units, where "Ar" designates a 4,4′-dibromobiphenyl linker, as well as oxygen-linked triaryltin sites $Ar_3Sn–O–SnAr_3$ (the hydrolysed $Ar_3Sn–OH$ sites were not detected) and alkylaryltin sites $^nBu_xAr_{(4-x)}Sn$ (incorporation of ^nBu groups is a result of the organometallic synthesis). A minor amount of SnO_2 (corresponding to *ca.* 5 wt% of the total tin content) was also identified. Formation of D-Man takes place *via* the Bilik mechanism, which is accompanied by a 1,2-shift of the carbon skeleton. Our recent results suggest that Ar_4Sn and $Ar_3Sn–O–SnAr_3$ structural units are the catalytically active sites for epimerization as shown by characterization of Sn-OF-1 in combination with catalytic data. Interestingly, the isomerization of D-Glc into D-Fru in the presence of Sn-OF-1 takes place following both the intramolecular hydride shift and the enediol formation mechanism. The carbon skeleton of D-Fru remains intact, which suggests isomerization of D-Glc into D-Fru and epimerization of D-Glc into D-Man catalyzed by Sn-OF-1 are parallel processes occurring *via* different mechanisms. SnO_2 and $^nBu_xAr_{(4-x)}Sn$ present minor structural elements of Sn-OF-1 and catalyze the isomerization of D-Glc into D-Fru.[20]

In this study, the acidity of Sn-OF-1 was analyzed by pyridine adsorption (Fig. S3). The difference spectra, after desorption exhibited the bands at 1608, 1580, 1487, 1477, and 1448 cm^{-1} which can be attributed to pyridine interacting with Lewis acid sites or with weak Brønsted acid sites (to give hydrogen-bonded Py-H sites) (Table S1).[42,43] No strong Brønsted acid sites are present, as judged by the absence of pyridinium bands at 1530–1550 cm^{-1} (Fig. S4). Molecular Sn(IV) compounds Ph_4Sn and $(Ph_3Sn)_2O$ structurally resembling previously uncovered catalytic active sites along with Ph_3SnOH were exposed to pyridine for

Open Access Article. Published on 17 September 2025. Downloaded on 2/13/2026 12:00:53 PM.
This article is licensed under a Creative Commons Attribution 3.0 Unported Licence.

comparison (Figs. S5 and S6). Notably, Ph_3SnOH shows a sharp negative band at 3600 cm^{-1} due to reaction of its Sn-OH sites.[42] Interestingly, this band is not present in the difference spectra of Sn-OF-1. Instead, there is a broad negative band at slightly lower wavenumbers, likely due to residual solvent in the porous structure. Thus, pyridine adsorption corroborates previously reported MAS NMR spectra suggesting the presence of Lewis acidic Sn^{4+} sites and the absence of Sn-OH sites.[20]

3.2. Epimerization of D-Glc catalyzed by Sn-OF-1

Kinetic profiles for D-Glc epimerization to D-Man were obtained for various temperatures, catalyst loadings, and reactant concentrations (Fig. S7–S15). Temperatures in the range of 80–100 °C were considered since degradation of the saccharides and lower mass balance was observed at higher temperatures.[19] Rates for reactant consumption (Tables S2 and S3) and product formation, determined from the initial slopes of the curves, are summarized in Table 1.

Under all of these conditions, the major reaction is the epimerization. Its rate depends linearly on the catalyst mass (Fig. S16). Reverse epimerization of D-Man to D-Glc was also studied (Fig. S17–S20). Reaction orders for both the forward (D-Glc to D-Man) and reverse (D-Man to D-Glc) reactions were determined from the slopes of the plots of log (initial reaction rate) *vs.* log (reactant concentration) (Fig. S21). The fractional reaction orders 0.56 ± 0.01 (forward) and 0.47 ± 0.01 (reverse) were calculated. Based on these observations, we propose eqn (1)–(3) to describe the reaction kinetics, based on the network in Fig. 3. D-Glc epimerization to D-Man is represented as a reversible reaction with forward rate constant ${k_1}^{G\rightarrow M}$ and reverse rate constant ${k_2}^{M\rightarrow G}$. Although one mole of D-Glc should yield one mole of D-Man, a gradual decrease in the mass balance over time indicates the formation of by-products (BP) (Fig. S22). Due to the higher concentration of D-Glc relative to D-Man, these by-products are assumed to originate predominantly from D-Glc, with

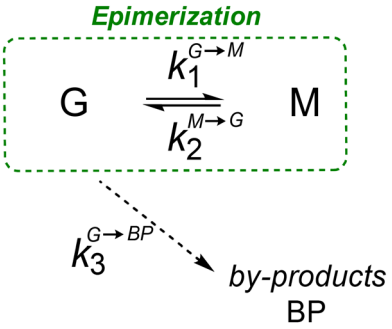

Fig. 3 Proposed reaction network for D-Glc (**G**) epimerization to D-Man (**M**) catalyzed by Sn-OF-1.

reaction rate constant ${k_3}^{G\rightarrow BP}$ and a simple first-order dependence on the concentration of D-Glc. In addition to the formation of by-products, the adsorption of the saccharides can cause a decrease in mass balance. We explored adsorption of D-Glc on Sn-OF-1 in the substrate concentration range of 1 to 10 wt% and observed *ca.* 10–15% uptake at room temperature (results not shown). Since adsorption is normally exothermic, we expect less uptake of the saccharides at elevated reaction temperatures.

$$\frac{dc_G}{dt} = -{k_1}^{G\rightarrow M}\cdot[\text{D-Glc}]^{0.56} + {k_2}^{M\rightarrow G}\cdot[\text{D-Man}]^{0.47} - {k_3}^{G\rightarrow BP}\cdot[\text{D-Glc}] \quad (1)$$

$$\frac{dc_M}{dt} = {k_1}^{G\rightarrow M}\cdot[\text{D-Glc}]^{0.56} - {k_2}^{M\rightarrow G}\cdot[\text{D-Man}]^{0.47} \quad (2)$$

$$\frac{dc_{BP}}{dt} = {k_3}^{G\rightarrow BP}\cdot[\text{D-Glc}] \quad (3)$$

The reaction was further explored by epimerizing 1-^{13}C-D-Glc at different temperatures. The ^{13}C label allows the reaction to be monitored using direct polarization solid-state NMR spectroscopy (Fig. 4 and S23–S25). Signals corresponding to

Table 1 Results of screening Sn-OF-1 for epimerization[a]

Entry	Reactant	T [°C]	c_{sugar} [wt%]	$m_{Sn\text{-}OF\text{-}1}$ [mg]	$r_{0,Epi}$ [mol L^{-1} min^{-1}]	TOF[b] [min^{-1}]	Ratio of monosaccharides			MB [%]
							D-Glc	D-Man	D-Fru	
1	D-Glc	80	10	100	2.5×10^{-3}	0.07	88	12	0	93
2	D-Glc	90	10	100	2.9×10^{-3}	0.08	85	15	1	95
3	D-Glc	100	10	100	4.8×10^{-3}	0.13	86	13	1	94
4	D-Glc	100	2	100	2.0×10^{-3}	0.06	71	26	4	91
5	D-Glc	100	5	100	3.6×10^{-3}	0.10	76	22	2	92
6	D-Glc	100	15	100	6.3×10^{-3}	0.18	82	17	1	89
7	D-Glc	100	10	70	3.9×10^{-3}	0.16	81	18	1	91
8	D-Glc	100	10	120	6.3×10^{-3}	0.25	80	17	3	92
9	D-Glc	100	10	150	7.5×10^{-3}	0.30	80	19	2	90
10	D-Man	100	2	100	2.0×10^{-3}	0.06	41	57	2	88
11	D-Man	100	5	100	3.1×10^{-3}	0.09	39	59	2	89
12	D-Man	100	10	100	4.4×10^{-3}	0.12	30	68	2	91
13	D-Man	100	15	100	5.0×10^{-3}	0.14	22	77	1	97

[a] $r_{0,Epi}$ is the initial rate of product formation; MB designates the mass balance. Reaction conditions: 5 mL EtOH : H_2O solution, 1.5 h, 750 rpm. [b] Turnover frequencies (TOFs) were calculated using eqn S1.

This journal is © The Royal Society of Chemistry 2026

Open Access Article. Published on 17 September 2025. Downloaded on 2/13/2026 12:00:53 PM.
This article is licensed under a Creative Commons Attribution 3.0 Unported Licence.

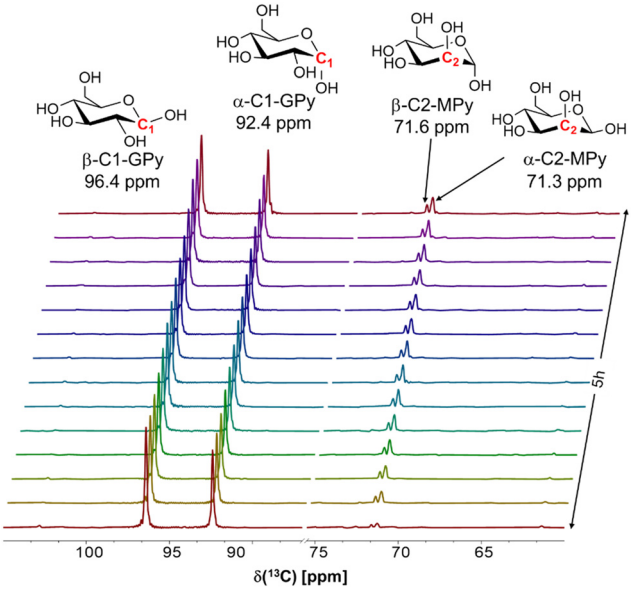

Fig. 4 Direct polarization MAS solid-state ^{13}C NMR (11.7 T, 3 kHz MAS) of Sn-OF-1 (9.4 mg) in the presence of a solution of 1-^{13}C-D-Glc in 50 : 50 wt% EtOH : H_2O (7.0 mol L^{-1}, 0.195 mL) at 92 °C. The time-resolved *operando* spectra show conversion of D-Glc to D-Man.

α-C1- and β-C1-glucopyranose (GPy) at 92.4 and 96.4 ppm, respectively, decrease monotonically over time. Simultaneously, peaks at 71.3 ppm and 71.6 ppm, corresponding to α-C2- and β-C2-mannopyranose (MPy), emerged, indicating the formation of 2-^{13}C-D-Man *via* a carbon shift from the C1 to the C2 position. Notably, the absence of signals at 94.1 and 93.7 ppm, typically associated with α-C1- and β-C1-MPy, excludes the possibility of a two-step isomerization *via* a D-fructose (D-Fru) intermediate.[19] Moreover, D-Fru was not detected since the spectra lack the resonances at 64.2 and 65.4 ppm corresponding to β-C1-fructofuranose and β-C1-fructopyranose, respectively. The β-/α-MPy ratio remained constant throughout the reaction (Fig. S26), indicating rapid equilibration of the two anomeric forms of D-Man.

Kinetic profiles were derived from the NMR spectra by integrating the total area under the carbohydrate signals as a function of time (Fig. S27). By fitting these profiles with the kinetic models represented by eqn (1)–(3), the rate constants $k_1^{G\rightarrow M}$, $k_2^{M\rightarrow G}$, and $k_3^{G\rightarrow BP}$ were determined at different temperatures (Table 2), and equilibrium constants were calculated as $K_{eq} = k_1^{G\rightarrow M}/k_2^{M\rightarrow G}$. Since the explored temperature range is narrow and the reaction exhibits a small reaction enthalpy change ΔH (Table 3), K_{eq} values do not vary significantly. Notably, for all tested temperatures, the equilibrium constant is slightly higher than those reported for aqueous solutions, $K_{eq}^{346-366K} = 0.34–0.38$,[44] likely due to the difference in solvent.

Using the Arrhenius equation (eqn S2), the activation energy and pre-factors were derived from Arrhenius plots of $\ln(k)$ *versus* $1/T$ (Fig. S28), with results summarized in Table 3. The activation barrier for epimerization of D-Glc into D-Man in the forward direction (69.9 kJ mol^{-1}) catalyzed by Sn-OF-1 is lower than those reported for molybdate catalysts (126 kJ mol^{-1} for ammonium heptamolybdate[45] and 97 kJ mol^{-1} for molybdenum-based polyoxometalates[12]) and metal–organic frameworks (MOFs) containing Lewis acid sites (88 kJ mol^{-1} for ZrMOF-808 (ref. 46) and 83 kJ mol^{-1} for UiO-66(Zr)[46]). The activation energy of the side reaction, 88 kJ mol^{-1}, exceeds both forward and reverse activation energies, implying that higher reaction temperatures reduce selectivity towards D-Man.[47]

The kinetic data offer insights into the optimal conditions for maximizing the yield and selectivity towards D-Man (Fig. S29 and S30). High selectivity was achieved across a range of reaction conditions (Fig. S30). However, at high D-Glc conversions, the selectivity for D-Man decreased, due to the increased prevalence of the by-product formation (Fig. S31). These changes correspond to the formation of by-products that are acidic, as confirmed by a slight decrease in pH (Fig. S32). Lower D-Glc concentrations favor increased selectivity for D-Man, while higher catalyst loadings reduce selectivity by accelerating the reaction rates for D-Glc consumption and D-Man formation, leading to a higher contribution of the side reactions (Table 2). The optimal conditions for maximizing both yield and selectivity of D-Man were identified as a D-Glc concentration of 5–10 wt%, 100 mg of Sn-OF-1 catalyst per 5 mL of solution, and a reaction temperature of 100 °C.

3.3. Purification of the D-Glc/D-Man mixture *via* adsorption by a CaY zeolite

The CaY zeolite was synthesized *via* ion exchange of commercial NaY zeolite using a $CaCl_2$ solution. The surface area of the zeolite marginally decreased after the ion exchange from 652 to 610 m^2 g^{-1} (Table S4). The micropore surface areas of CaY and NaY zeolites are 550 and 605

Table 2 Rate constants and equilibrium constants for epimerization at different temperatures,[a] calculated from time-resolved *operando* MAS NMR results

Entry	T [°C]	$k_1^{G\rightarrow M}$ [h^{-1}]	$k_2^{M\rightarrow G}$ [h^{-1}]	$k_3^{G\rightarrow BP}$ [h^{-1}]	K_{eq}
1	73	0.13 ± 0.02	0.35 ± 0.04	0.007 ± 0.002	0.4 ± 0.1
2	83	0.25 ± 0.06	0.63 ± 0.08	0.024 ± 0.002	0.4 ± 0.1
3	88	0.31 ± 0.04	0.8 ± 0.2	0.033 ± 0.008	0.4 ± 0.1
4	92	0.47 ± 0.06[1]	1.1 ± 0.3	0.033 ± 0.002	0.4 ± 0.2

[a] Reaction conditions: Sn-OF-1 (9.4 mg), 1-^{13}C-D-Glc in 50 : 50 wt% EtOH : H_2O (7.12 mol L^{-1}, 0.195 mL).

Open Access Article. Published on 17 September 2025. Downloaded on 2/13/2026 12:00:53 PM.
This article is licensed under a Creative Commons Attribution 3.0 Unported Licence.

Table 3 Activation energies and the epimerization enthalpy ΔH

Entry	Reaction	E_A [kJ mol^{-1}]	$\Delta H = E_{A,1} - E_{A,2}$ [kJ mol^{-1}]
1	D-Glc → D-Man	70 ± 5	11.8
2	D-Man → D-Glc	58 ± 5	
3	By-product formation	88 ± 5	

m^2 g^{-1}, respectively, indicating that the pore structure was preserved. The Si/Al ratio of the parent NaY zeolite, 2.8, remained unchanged after $CaCl_2$ treatment. The chlorine content of 0.03 wt% confirmed the effective removal of $CaCl_2$ by washing (Table S5). The ion-exchange process resulted in approximately 77% Na^+ substitution by Ca^{2+}. SEM analysis revealed well-defined square particles of 900–1000 nm, with no significant morphological changes upon ion exchange (Fig. S33). XRD analysis indicated that the crystal structure of the zeolite was retained (Fig. S34).

Individual isotherms for adsorption of D-Glc and D-Man on CaY zeolite, analyzed using the Langmuir model (eqn S6), are shown in Fig. 5. Table 4 summarizes the corresponding maximum loadings q_{max}, Langmuir constants $K_{Langmuir}$, along with the Henry constants K_{Henry} determined by linearization of the curves at low sugar concentrations (Fig. S35). It was not possible to explore higher sugar concentrations due to limited solubility of the substrates in water–ethanol mixtures.

Adsorption is fast, with equilibrium being reached in less than 5 min (Fig. S36). The extent of adsorption depends significantly on the solvent composition: in pure water, nearly no sorption was observed, whereas an increase in fraction of ethanol resulted in a dramatic increase in the adsorption capacity. Fornefett *et al.* explored sucrose adsorption on Y zeolites from water–ethanol mixtures, reporting significantly higher sucrose loading from a water–ethanol mixture than from pure water. The effect was attributed to the hydrophilicity of the zeolite: by increasing the fraction of ethanol, the competition between water and saccharide for adsorption sites was reduced, allowing the zeolite to adsorb a significantly higher amount of sugar.[33] In addition, the stability of Ca^{2+} complexes of saccharides increases upon addition of an organic co-solvent.[23,48] Water efficiently desorbed the individually adsorbed D-Glc and D-Man: 78–95% of each adsorbed saccharide was recovered (Table 5). A somewhat lower D-Man desorption rate of 78% was observed when the material was dried after the adsorption step prior to the desorption (entry 3 in Table 5). When the drying process was omitted, 95% of D-Man was recovered by the adsorption (entry 4 in Table 5). This result can be explained by a partial degradation of D-Man coordinated to Ca^{2+} cation during the drying of the CaY zeolite at elevated temperature.

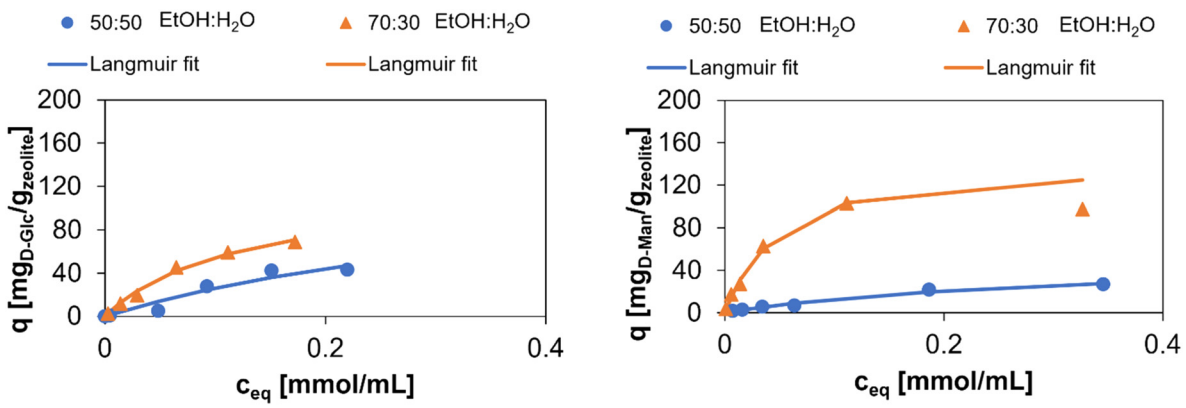

Fig. 5 Adsorption isotherms for individually adsorbed D-Glc (left) and D-Man (right) on CaY zeolites at different EtOH : H_2O ratios. Adsorption conditions: 500 mg zeolite, 3 mL EtOH : H_2O solution, 2 h, RT, 500 rpm.

Table 4 Results from individual sorption isotherms for D-Glc and D-Man, recorded for various solvent compositions[a]

			Henry model	Langmuir model		
Entry	Reactant	EtOH : H_2O	K_{Henry}	q_{max} [mg$_{sugar}$ g$_{zeolite}^{-1}$]	$K_{Langmuir}$	R^2
1	D-Glc	50 : 50	254	141	2.3	0.93
2	D-Man	50 : 50	119	52	3.3	0.98
3	D-Glc	70 : 30	701	120	8.4	0.99
4	D-Man	70 : 30	2104	116	30	0.99

[a] Adsorption conditions: 500 mg zeolite, 3 mL EtOH : H_2O solution, 2 h, RT, 500 rpm.

This journal is © The Royal Society of Chemistry 2026

Open Access Article. Published on 17 September 2025. Downloaded on 2/13/2026 12:00:53 PM.
This article is licensed under a Creative Commons Attribution 3.0 Unported Licence.

Table 5 Results of desorption experiments for individually adsorbed D-Glc and D-Man[a]

Entry	Reactant	q [$mg_{sugar}\ g_{zeolite}^{-1}$]	Adsorption [%]	Desorption [%]
1	D-Glc[b]	68	29	90
2	D-Glc[c]	66	28	85
3	D-Man[b]	96	43	78
4	D-Man[c]	94	41	95

[a] Adsorption conditions: 500 mg CaY, 3 mL sugar solution (50 mg g^{-1}) in 70 : 30 wt% EtOH : H_2O, 2 h, 500 rpm, RT. Desorption conditions: 3 mL H_2O, 1 h, 500 rpm, RT. [b] After adsorption, the zeolite was dried in an oven at 80 °C. [c] Without drying the zeolite after adsorption.

Competitive adsorption of D-Glc and D-Man over CaY zeolite was studied in a 70 : 30 wt% EtOH : H_2O solvent mixture. Fig. 6 shows the competitive adsorption isotherms over CaY zeolites, while Table 6 summarizes the adsorption parameters obtained by curve fitting as well as the separation factors (SF) calculated using eqn S9. Henry's Law constants for the adsorption of D-Man are significantly higher than for the adsorption of D-Glc at sugar ratios of 80 : 20 or 50 : 50 (Fig. S37). Interestingly, the selectivity for D-Man adsorption increases at the lower concentration of D-Glc, with SF values of 1.5 and 3.2 for solutions with 80 : 20 and 50 : 50 ratios, respectively.

Water was used to desorb D-Glc and D-Man adsorbed from a mixture with 67 : 33 ratio of the saccharides. Rinsing the loaded zeolite twice with water resulted in recovery of 70% D-Man and 98% D-Glc. Stirring the zeolite after rinsing led to further recovery of 1% D-Man (Table S5). Thus, desorption with water is quick and efficient.

3.4. Combination of catalysis by Sn-OF-1 with crystallization and adsorption

Catalytic synthesis of D-Man over Sn-OF-1 was combined with separation of the product. D-Man was synthesized using Sn-OF-1 at 100 °C from a 5 wt% D-Glc solution under the optimized reaction conditions (Fig. 7). After the epimerization, the reaction solution contained 21% D-Glc and 68% D-Man estimated based on the carbon balance, which corresponded to a 77 : 23 ratio of D-Clc : D-Man. Next, a portion of D-Glc was removed from the solution *via* crystallization. Several solvents were reported in literature to achieve selective crystallization of D-Glc from its mixture with D-Man.[6] The following liquids were tested in this study as antisolvents: 4.7 : 1 and 1 : 1 ethanol-to-methanol as well as pure ethanol. The highest yield of crystallized D-Glc, obtained with the 4.7 : 1 ethanol-to-methanol mixture, corresponded to recovery of *ca.* 73% of the dissolved Glc with a purity of 96–98% (Table S7 and Fig. S38 and S39). The amount of D-Glc

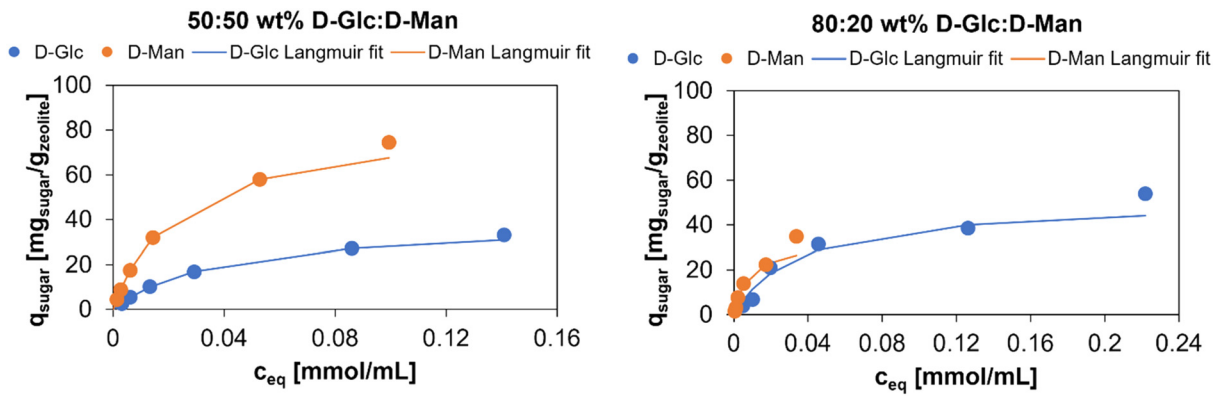

Fig. 6 Competitive adsorption of D-Glc and D-Man by CaY zeolites. Adsorption conditions: 500 mg zeolite, 3 mL 70 : 30 wt% EtOH : H_2O solution, 2 h, RT, 500 rpm.

Table 6 Results of competitive sorption isotherms for adsorption of sugars by CaY zeolite[a]

Entry	Zeolite	Sugar	Sugar ratio D-Glc : D-Man	Henry model K_{Henry}	Langmuir model q_{max} [$mg_{sugar}\ g_{zeolite}^{-1}$]	Langmuir model $K_{Langmuir}$	Langmuir model R^2	SF
1	CaY	D-Glc	50 : 50	796	40	26	0.99	3.2
		D-Man		2955	83.2	43	1.00	
2	CaY	D-Glc	80 : 20	981	51.3	28.4	0.98	1.5
		D-Man		2788	32.3	133.8	0.99	

[a] Adsorption conditions: 500 mg zeolite, 3 mL 70 : 30 wt% EtOH : H_2O solution, 2 h, RT, 500 rpm.

Open Access Article. Published on 17 September 2025. Downloaded on 2/13/2026 12:00:53 PM.
This article is licensed under a Creative Commons Attribution 3.0 Unported Licence.

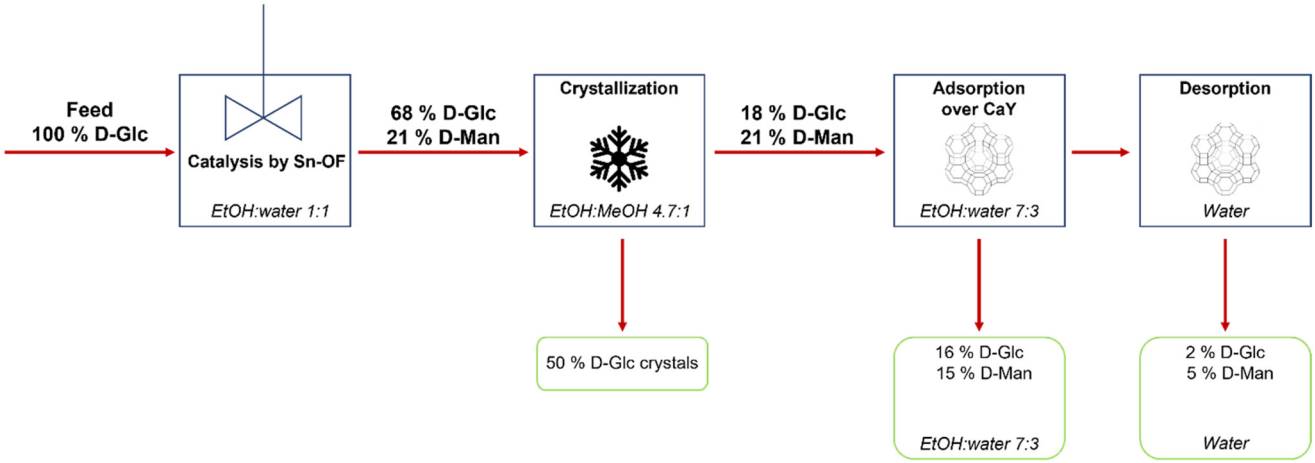

Fig. 7 Synthesis and isolation of D-Man *via* epimerization of D-Glc in the presence of Sn-OF-1 followed by recovery of D-Man by adsorptive separation over CaY zeolite. Percent values reflect the carbon balance.

recovered by crystallization refers to *ca.* 50% of the initially loaded substrate. The obtained crystallized D-Glc was successfully epimerized in the presence of Sn-OF-1 (Table S8 and Fig. S40).

After the crystallization step, the sugar solution contained 18% D-Glc and 21% D-Man when calculating the carbon balance to the initially loaded substrate. This mixture was dissolved in a 70 : 30 wt% mixture of ethanol and water for adsorption by CaY zeolite followed by desorption into water. Two liquid fractions were obtained: (1) the remaining supernatant, containing *ca.* 75% D-Man with a purity of *ca.* 50% (in Fig. 7, 16% D-Glc and 15% D-Man in EtOH : water 7 : 3), and (2) the desorption solution, containing *ca.* 25% D-Man with a purity of *ca.* 70% (in Fig. 7, 2% D-Glc and 5% D-Man in water). As Fig. 7 depicts, the approach results in recovery of crystalline D-Glc and two liquid fractions enriched with D-Man. The proposed separation method can be further developed by transferring into a continuous mode and performing a column separation. The data on adsorption in water and in water-ethanol mixtures will contribute to designing a gradient elution. Moreover, simulated moving bed (SMB) presents an attractive possibility to perform the separation of the binary mixture of D-Glc and D-Man in a continuous manner.[49]

4. Conclusions

This study demonstrates that Sn-OF-1 is a highly effective chemo-catalyst for the epimerization of D-Glc to D-Man, offering a feasible and efficient approach for producing D-Man under mild reaction conditions. The kinetic analyses reveal the optimal conditions—temperature, catalyst loading, and reactant concentration—to enhance selectivity towards D-Man. With an activation energy of 70 kJ mol^{-1}, Sn-OF-1 exhibits an activity comparable to state-of-the-art catalysts, showing its potential for industrial applications.

Additionally, this work introduces a strategy for separating D-Glc and D-Man mixtures resulting from epimerization. The approach combines (1) partial recovery of unconverted D-Glc and (2) purification of D-Man. Adsorptive separation using CaY zeolite proved to be a simple and time-efficient method, employing water-ethanol and water as the adsorption and desorption solvents, respectively. Notably, the adsorbed sugars are desorbed rapidly without additional workup. The combination of Sn-OF-1 catalysis, crystallization, and adsorptive separation with CaY zeolites represents a promising pathway for the scalable synthesis of D-Man.

Author contributions

Valérie Toussaint: conceptualization, methodology, validation, investigation (synthesis and characterization, performing catalytic experiments, adsorption experiments), visualization, writing – original draft, writing – review & editing; Loretta Pavlis: investigation (performing adsorption and desorption experiments), writing – review & editing; Pia Groß: investigation (synthesis and characterization, performing catalytic experiments), writing – review & editing; Samantha Ausman: conceptualization, methodology (*operando* solid-state NMR spectroscopy), writing – review & editing; Karin Föttinger: instrumentation, writing – review & editing; Susannah Scott: methodology, supervision (*operando* solid-state NMR spectroscopy), writing – review & editing; Irina Delidovich: conceptualization, methodology, validation, funding acquisition, project administration, writing – original draft, writing – review & editing.

Conflicts of interest

There are no conflicts to declare.

Data availability

Supplementary information: Supplementary information (SI) includes characterization data for Sn-OF-1 and CaY zeolite (N_2 physisorption, XRD, XRF, IR spectra of pyridine adsorption, SEM), results of catalytic results of Sn-OF-1 for

 This journal is © The Royal Society of Chemistry 2026

Open Access Article. Published on 17 September 2025. Downloaded on 2/13/2026 12:00:53 PM. This article is licensed under a Creative Commons Attribution 3.0 Unported Licence.

conversion of D-glucose, details of the kinetic study, adsorption/desorption profiles, details of the crystallization experiments, and all relevant calculations. See DOI: **https://doi.org/10.1039/D5RE00314H**.

We hereby confirm that the data underlying the reported research are available in the article itself and in the submitted SI.

Acknowledgements

We thank Jerry Hu and Jaya Nolt for their assistance with NMR spectroscopy and Jason Chalmers for his invaluable help and insightful discussions, particularly with data fitting. We acknowledge the support provided by Prof. Regina Palkovits and Dr. Tobias Riedl throughout this project. We thank Helga Seidelmann and Thomas Jung for HPLC analysis. We are grateful for the resources and facilities provided by the X-ray Center (XRC) at TU Wien.

Financial support of the Deutsche Forschungsgemeinschaft (DFG, German Research Foundation) – Project number 450360023 – is greatly appreciated. V. T. thanks the Austrian Marshall Plan Foundation for an academic exchange program scholarship. Financial support for the NMR measurements from the U.S. Department of Energy, Office of Science, Division of Basic Energy Sciences, under the Catalysis Science Initiative (DE-FG-02-03ER15467) is gratefully acknowledged. Part of this work was done in the MRL Shared Experimental Facilities, which are supported by the MRSEC Program of the NSF under Award No. DMR 2308708; a member of the NSF-funded Materials Research Facilities Network. The authors acknowledge TU Wien Bibliothek for financial support through its Open Access Funding Programme.

References

1 H. Wu, W. Zhang and W. Mu, *Appl. Microbiol. Biotechnol.*, 2019, **103**, 8753–8761.
2 X. Hu, Y. Shi, P. Zhang, M. Miao, T. Zhang and B. Jiang, *Compr. Rev. Food Sci. Food Saf.*, 2016, **15**, 773–785.
3 H. Schiweck, A. Bär, R. Vogel, E. Schwarz, M. Kunz, C. Dusautois, A. Clement, C. Lefranc, B. Lüssem, M. Moser and S. Peters, Sugar Alcohols, in *Ullmann's Encyclopedia of Industrial Chemistry*, 2012, DOI: **10.1002/14356007.a25_413.pub3**.
4 M. Makkee, A. Kieboom and H. Van Bekkum, *Starch-Stärke*, 1985, **37**, 136–141.
5 D.-M. Gao, X. Zhang, H. Liu, H. Fujino, T. Lei, F. Sun, J. Zhu and T. Huhe, *Green Energy Environ.*, 2023, **9**, 435–453.
6 V. Bilik, *Chem. Zvesti*, 1972, **26**, 183–186.
7 K. Hashimoto, T. Niina, T. Kobayashi, S. Adachi and Y. Watanabe, *Carbohydr. Res.*, 2024, **535**, 109003.
8 C. Han, J.-J. Ji, H. Xia and B. Fei, *New J. Chem.*, 2024, **48**, 11674–11681.
9 S. Luo, M. A. Alam, D. Gao, Y. Li, L. Zhao, M. Xu, J. Xu and S. Zhang, *Biomass Convers. Biorefin.*, 2025, **15**, 20949–20961.
10 A. Köckritz, M. Kant, M. Walter and A. Martin, *Appl. Catal., A*, 2008, **334**, 112–118.
11 P. Zhu, S. Meier and A. Riisager, *Appl. Catal., A*, 2024, **687**, 119976.
12 F. Ju, D. VanderVelde and E. Nikolla, *ACS Catal.*, 2014, **4**, 1358–1364.
13 M. Ventura, J. A. Cecilia, E. Rodríguez-Castellón and M. E. Domine, *Green Chem.*, 2020, **22**, 1393–1405.
14 I. Delidovich and R. Palkovits, *ChemSusChem*, 2016, **9**, 547–561.
15 V. Bilik, *Chem. Zvesti*, 1972, **26**, 372–375.
16 J. Wan, P. Chu, X. Wang, Z. Sun, W. Zhang, Y. Wang, Q. Zhang, W. Yan, X. Jin and C. Yang, *ACS Sustainable Chem. Eng.*, 2024, **12**, 14940–14951.
17 H. Hu, S. Liu, W. Zhang, J. An and H. Xia, *ChemistrySelect*, 2020, **5**, 1728–1733.
18 S. M. Arumugam, S. Mahala, B. Devi, S. Kumar, R. K. Kunchala and S. Elumalai, *React. Chem. Eng.*, 2023, **8**, 2641–2657.
19 I. Delidovich, A. Hoffmann, A. Willms and M. Rose, *ACS Catal.*, 2017, **7**, 3792–3798.
20 V. Toussaint, S. Bachmann, A.-C. Pöppler, V. L. Sushkevich, G. Friedbacher, T. Konegger, L. Brunnbauer, A. Limbeck, C. Hametner, G. Rupprechter and I. Delidovich, *J. Catal.*, 2025, **447**, 116130.
21 V. Toussaint, T. Röper, K. Hricova and I. Delidovich, *Curr. Opin. Green Sustainable Chem.*, 2025, **11**, 100476.
22 I. Delidovich and V. Toussaint, *Green Chem.*, 2024, **26**, 720–738.
23 S. J. Angyal, G. S. Bethell and R. J. Beveridge, *Carbohydr. Res.*, 1979, **73**, 9–18.
24 J. P. Sherman and C. C. Chao, in *Studies in Surface Science and Catalysis*, Elsevier, 1986, vol. 28, pp. 1025–1032.
25 R. Schöllner, W.-D. Einicke and B. Gläser, *J. Chem. Soc., Faraday Trans.*, 1993, **89**, 1871–1876.
26 H. Caruel, L. Rigal and A. Gaset, *J. Chromatogr. A*, 1991, **558**, 89–104.
27 J. Tiihonen, I. Markkanen and E. Paatero, *Chem. Eng. Commun.*, 2002, **189**, 995–1008.
28 C. Ho, C. B. Ching and D. M. Ruthven, *Ind. Eng. Chem. Res.*, 1987, **26**, 1407–1412.
29 C. B. Ching, C. Ho, K. Hidajat and D. M. Ruthven, *Chem. Eng. Sci.*, 1987, **42**, 2547–2555.
30 C. B. Ching and D. M. Ruthven, *Zeolites*, 1988, **8**, 68–73.
31 P. K. Muralidharan and C. B. Ching, *Ind. Eng. Chem. Res.*, 1997, **36**, 407–413.
32 R. C. Kuhn and F. M. Filho, *J. Chromatogr., B*, 2010, **878**, 2023–2028.
33 I. Fornefett, D. Rabet, C. Buttersack and K. Buchholz, *Green Chem.*, 2016, **18**, 3378–3388.
34 C. Buttersack, I. Fornefett, J. Mahrholz and K. Buchholz, in *Studies in Surface Science and Catalysis*, ed. H. Chon, S.-K. Ihm and Y. S. Uh, Elsevier, 1997, vol. 105, pp. 1723–1730.
35 C. Buttersack, W. Wach and K. Buchholz, *J. Phys. Chem.*, 1993, **97**, 11861–11864.
36 M. Francisco, A. N. Mlinar, B. Yoo, A. T. Bell and J. M. Prausnitz, *J. Chem. Eng.*, 2011, **172**, 184–190.

Open Access Article. Published on 17 September 2025. Downloaded on 2/13/2026 12:00:53 PM.
This article is licensed under a Creative Commons Attribution 3.0 Unported Licence.

37 W. Ammar, K. Larmier, A. Methivier and M. Manko, *Sep. Purif. Technol.*, 2025, **354**, 128784.
38 J. P. Sherman and C. C. Chao, Carbohydrate Separations Using Zeolite Molecular Sieves, in *Studies in Surface Science and Catalysis*, ed. Y. Murakami, A. Iijima and J. W. Ward, Elsevier, 1986, pp. 1025–1032, DOI: **10.1016/S0167-2991(09)60978-2**.
39 E. D. Walter, L. Qi, A. Chamas, H. S. Mehta, J. A. Sears, S. L. Scott and D. W. Hoyt, *J. Phys. Chem. C*, 2018, **122**, 8209–8215.
40 L. Qi, R. Alamillo, W. A. Elliott, A. Andersen, D. W. Hoyt, E. D. Walter, K. S. Han, N. M. Washton, R. M. Rioux, J. A. Dumesic and S. L. Scott, *ACS Catal.*, 2017, **7**, 3489–3500.
41 V. Toussaint and I. Delidovich, *Catal. Sci. Technol.*, 2022, **12**, 4118–4127.
42 L. H. Wee, T. Lescouet, J. Fritsch, F. Bonino, M. Rose, Z. Sui, E. Garrier, D. Packet, S. Bordiga, S. Kaskel, M. Herskowitz, D. Farrusseng and J. A. Martens, *Catal. Lett.*, 2013, **143**, 356–363.
43 C. Morterra and G. Magnacca, *Catal. Today*, 1996, **27**, 497–532.
44 M. Liu, Y. He, Y.-Y. Jiao, L. Ding, D. An, Y. Yang, Q.-Q. Hao, H.-Y. Chen and Q.-X. Luo, *ACS Catal.*, 2024, **14**, 14895–14911.
45 A. Cybulski, B. Kuster and G. Marin, *J. Mol. Catal.*, 1991, **68**, 87–103.
46 S. Rojas-Buzo, A. Corma, M. Boronat and M. Moliner, *ACS Sustainable Chem. Eng.*, 2020, **8**, 16143–16155.
47 C. Li, Y. Wang, Y. Zhang, M. Wang, X. Sun, H. Cui and Y. Xie, *ChemistrySelect*, 2020, **5**, 270–279.
48 J. Tiihonen, I. Markkanen and E. Paatero, *Chem. Eng. Commun.*, 2002, **189**, 995–1008.
49 F. D. Antia and C. Horváth, *J. Chromatogr. A*, 1989, **484**, 1–27.

This journal is © The Royal Society of Chemistry 2026